Available online at www.sciencedirect.com
SCIENCE DIRECT®
Sensors and Actuators B 113 (2006) 169–176
SENSORS AND ACTUATORS B CHEMICAL
www.elsevier.com/locate/snb

Design and fabrication of an alternating dielectric multi-layer device for surface plasmon resonance sensor

Chii-Wann Lin [a,b,f,*], Kuo-Ping Chen [a], Chien-Nan Hsiao [c], Shiming Lin [d], Chih-Kung Lee [e]

[a] *Institute of Biomedical Engineering, College of Engineering and College of Medicine, National Taiwan University, No. 1, Sec. 1, Ren-Ai Road, Taipei 100, Taiwan*
[b] *Department of Electrical Engineering, College of Electrical Engineering and Computer Science, National Taiwan University, No. 1, Sec. 4, Roosevelt Road, Taipei 106, Taiwan*
[c] *Precision Instrument Development Center, National Science Council, 20 R&D Road VI, Hsinchu Science Park, Hsinchu 300, Taiwan*
[d] *Center for Optoelectronic Biomedicine, College of Medicine, No. 1, Sec. 1, Ren-Ai Road, Taipei 100, Taiwan*
[e] *Institute of Applied Mechanics, College of Engineering, National Taiwan University, No. 1, Sec. 4, Roosevelt Road, Taipei 106, Taiwan*
[f] *Center for Nano Science and Technology, National Taiwan University, No. 1, Sec. 4, Roosevelt Road, Taipei 106, Taiwan*

Received 13 April 2004; received in revised form 11 February 2005; accepted 21 February 2005
Available online 16 March 2005

Abstract

An alternating dielectric multi-layer device was fabricated and tested in the laboratory to show that dielectric mirrors of alternating high/low refractive index materials, based on the design of distributed Bragg reflector (DBR) for vertical cavity surface emission lasers (VCSELs), can be used in designing SPR biochemical sensors. The thickness, number of layers, and other design parameters of the device used were optimized using optical admittance loci analysis. The proof-of-concept device was fabricated with a symmetrical structure using Au/$(SiO_2/TiO_2)_4$/Au.

Using a 632 nm-wavelength light source on a BK7 coupling prism, our laboratory tests showed that, under water, there was an 11.5° shift in resonant peak position towards the critical angle (from 74° in a conventional single-layer Au film), and a 3.25 times decrease in FWHM (the half-peak width). Our design also resulted in a wider dynamic range of up to a 1.50 refractive index unit (RIU), compared to 1.38 RIU in a conventional single-layer Au film. Using glucose solutions in ddH_2O, the calculated resolution was 1.28×10^{-5}. The calculated intensity sensitivity was 10 000 a.u./RIU, about twice the improvement over the conventional single-layer Au film.

Keywords: Surface plasmon resonance; Dielectric mirror; Admittance loci; Biosensor

1. Introduction

The behavior of free electrons or plasma near the interface of a metallic-dielectric material has been widely studied. It is known that high-density electron gas, when subject to collective longitudinal excitation or oscillation, will manifest particle behavior. Analogous to phonos, magnons and excitons, the phenomenon has been called "plasmon" [1,2]. This phenomenon was first observed in metal grating in the early 1900s. Kretschmann used a metallic-film-coated (∼50 nm) prism to generate a surface plasmon resonance (SPR) signal [3]. Since then, the Kretschmann prism-coupling device has been used extensively to study the optical properties of metallic thin films, including index of refraction (n), extinction coefficient (k), thickness (d), and roughness [4].

Typically, light or electrons is used to generate a surface-localized electromagnetic wave [5]. The electric field is strongest at the interface, and diminishes exponentially along the sides of the penetration distance from the interface. The SPR signal can be used to probe the vicinity of the metallic–dielectric interface, in the range of several hundred nanometers. However, the generation of the SPR signal must satisfy the following conditions: (1) the real part of the

* Corresponding author. Tel.: +886 2 3366 5272; fax: +886 2 3366 5268.
E-mail address: cwlinx@ntu.edu.tw (C.-W. Lin).

0925-4005/$ – see front matter © 2005 Elsevier B.V. All rights reserved.
doi:10.1016/j.snb.2005.02.044

complex dielectric constant of the surface active medium must be negative (such as Au or Ag), and (2) momentum matching between the excitation and the plasmon resonance is required [6].

With a Kretschmann prism-coupling device, at an angle depending on the metal and the surrounding medium, the lowest point on the TM-wave reflectance curve can be located. The changes in reflective intensity are recorded as the SPR spectra. The SPR signal is highly sensitive to the optical properties of the dielectric material (e.g. bio-molecules) adjacent to the surface of the metallic firm. Monitoring the shift in SPR signal (the presence of immobilized or captured molecules) can be used in the design of SPR biochemical sensors.

The unique characteristics of non-labeling and real-time monitoring can be used in many biochemical and biophysical applications [7–13], for both prism- and fiber-based systems [14,15]. However, it is observed that using a 632 nm-wavelength light source on a BK7 coupling prism, an SPR device with a metallic–dielectric material immersed in water would produce a large resonant angle (about 74°). This can cause image distortion and difficulties in optical alignment during angle scanning measurements. Considering the optical system, a solution is to use a near-infrared light source, or to use a higher refractive index coupling prism to lower the resonant angle and sharpen the SPR curve [16]. Alternative approaches, based on the use of dielectric materials and structural design [17], include long-range surface plasmon resonance (LRSPR) [18,19], coupled plasmon waveguide resonance (CPWR) [20], or a combination of both configurations.

Traditionally, multi-layer dielectric materials are fabricated in quarter or half wavelength thickness, and are used in highly selective transmission or with reflectance within a specific range of wavelength. The intrinsic optical properties in multi-layer dielectric materials and the interference phenomenon are the basis for using a distributed Bragg reflector (DBR) to achieve a desired quality of resonance. This interference phenomenon is often used to improve performance of many optical coatings.

The purpose of our research is to determine whether or not dielectric mirrors of alternating high/low refractive index materials, based on the design of DBR for vertical cavity surface emission lasers (VCSELs) [21], can be used in designing SPR biochemical sensors. We designed and fabricated a multi-layer device to modulate the SPR signal, without changing the light source or coupling prism. The proof-of-concept device and the test results, along with brief explanations of the admittance loci design method, are given in the next section.

2. Materials and methods

2.1. SPR and equivalent admittance of thin film

Detailed discussions of surface plasmon near the interface of a metallic medium and a dielectric medium can be found widely in the literature [2,3]. It is known that the continuity of a p-polarized electric field at an interface normal to a z-direction will induce fluctuations in surface charges, otherwise known as surface plasmon waves. On a metal with negative dielectric constant ε_2 and a dielectric material with positive dielectric constant ε_1, the E_z electric field at the interface will have two opposite propagating directions. This results in fluctuation of the surface charge density, and macroscopic oscillation of electric field in the two media. Both electric fields have components oscillating along the x- and the z-directions. Since the surface density alternates in sign, the spatial summation in the z-direction results in an exponential decay in electric field. The positive dielectric material mentioned here can be multi-layered. To calculate its reflectance and transmittance, the device can be studied theoretically as an equivalent single-layer device. In this paper, we direct our research on the oblique incidence of the electromagnetic waves, as this is more relevant to the SPR devices of interest.

2.1.1. Single interface

The refractive index of a light beam propagating on a medium is $N = c/v$, where constant c is the velocity of light in a vacuum, and v is the light speed in the material. This can also be expressed as $n - ik$, where the real number n is the refractive index, and the imaginary part k is the extinction coefficient. Fig. 1(a) shows the interface of two materials with respective complex refractive indices N_0 and N_1, where the light beams obliquely from N_0 to N_1.

The total E field and H field can be expressed as

$$E_{0\mathrm{I}}^{+} + E_{0\mathrm{r}}^{-} = E_{1\mathrm{T}}^{+}, \qquad H_{0\mathrm{I}}^{+} - H_{0\mathrm{r}}^{-} = H_{1\mathrm{T}}^{+} \tag{1}$$

Note that the direction of the E field along $E_{\|}$ and $H_{\|}$ is continuous at the boundary, where a positive value ("+") is designated as the incident direction, and a minus value ("−") is designated as the opposite direction. Furthermore, let "I" represent the incident direction, "r" the reflected position and "T" the transmitted direction. The optical admittance, y, is

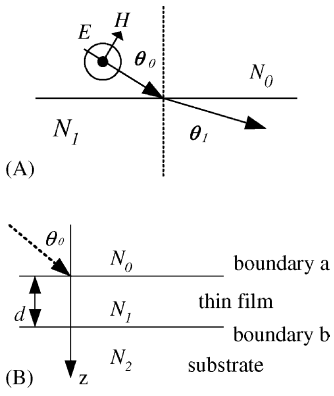

Fig. 1. Schematic diagram and notation used for theoretical analysis at the interface of (a) two different materials, which have complex refractive indices N_0 and N_1; (b) multi-layer with thin film thickness d with refractive index N_1 on substrate with refractive index N_2. The light beam is obliquely incident from N_0 to N_1, the E field direction is out of the paper, and the H field is continuous at the boundary.

defined as

$$y = \frac{H}{E} \tag{2}$$

Combining Eqs. (1) and (2), the amplitude of the reflection coefficient ρ becomes

$$\rho = \frac{E_{0r}^{-}}{E_{0I}^{+}} = \frac{y_0 - y_1}{y_0 + y_1} \tag{3}$$

The optical admittance $y = NY_0$, where Y_0 is the free space admittance. $Y_0 = 1/377$ simems. The reflectance is

$$R = \rho\rho^* = \left(\frac{N_0 - N_1}{N_0 + N_1}\right)^2 \tag{4}$$

As shown in Fig. 1(a), when a light beam strikes obliquely at angle θ_0, the refractive angel θ can be calculated using Snell's Law as

$$N_0 \sin\theta_0 = N_1 \sin\theta \tag{5}$$

At different polarization states, the optical admittance of an obliquely incident light beam changes to

$$\text{p-wave (TM)}: \ \eta_p = \frac{H}{E\cos\theta} = \frac{N}{\cos\theta}x \tag{6}$$

$$\text{s-wave (TE)}: \ \eta_s = \frac{H\cos\theta}{E} = N\cos\theta \tag{7}$$

The reflectance at the interface can be determined by inserting the above into Eq. (3), i.e. $y \to \eta$.

2.1.2. Multiple interfaces

For a multi-layer device, we first consider the reflectance of a thin film (N_1) on a substrate (N_2). The relationship of E and H at the boundaries of a and b, as shown in Fig. 1(b) is

$$E_{a1}^{+} = E_{b1}^{+}\,e^{i\delta_1}, \qquad H_{a1}^{+} = H_{b1}^{+}\,e^{i\delta_1}; \qquad E_{a1}^{-} = E_{b1}^{-}\,e^{-i\delta_1},$$
$$H_{a1}^{-} = H_{b1}^{-}\,e^{-i\delta_1} \tag{8}$$

The "+" sign means it is along the positive z-direction, the "−" sign designates the opposite direction, and δ_1 is the phase factor due to thin film layer 1. The phase factor is a function of the refractive index, thickness, incident angle and wavelength. This is defined as

$$\delta_1 = \frac{2\pi N_1 d\cos\theta_1}{\lambda} \tag{9}$$

Therefore, Eq. (8) can be rewritten either as

$$E_a = E_{b1}^{+} + E_{b1}^{-} = E_b\cos\delta_1 + \frac{iH_b}{\eta_1}\sin\delta_1,$$
$$H_a = H_{b1}^{+} + E_{b1}^{-} = i\eta_1 E_b\sin\delta_1 + H_b\cos\delta_1 \tag{10}$$

In matrix form:

$$\begin{bmatrix} E_a \\ H_a \end{bmatrix} = \begin{bmatrix} \cos\delta_1 & i\sin\delta_1/\eta_1 \\ i\eta_1\sin\delta_1 & \cos\delta_1 \end{bmatrix} \begin{bmatrix} E_b \\ H_b \end{bmatrix} \tag{11}$$

The above 2×2 matrix is known as the characteristic matrix (M_1) of the thin film. We define the equivalent admittance (Y_e) as

$$Y_e = \frac{H_a}{E_a} \tag{12}$$

Let $Y_e = C/B$. Eq. (12) becomes

$$\begin{bmatrix} B \\ C \end{bmatrix} = \begin{bmatrix} \cos\delta_1 & i\sin\delta_1/\eta_1 \\ i\eta_1 \sin\delta_1 & \cos\delta_1 \end{bmatrix} \begin{bmatrix} 1 \\ \eta_2 \end{bmatrix} \tag{13}$$

With this equivalent admittance, determining the reflectance of a multiple layer device on a substrate is similar to the single-layer case. As shown in Fig. 2(a), the characteristic matrix can likewise be used to obtain an equivalent admittance and reflectance:

$$\begin{bmatrix} E_a \\ H_a \end{bmatrix} \Rightarrow \begin{bmatrix} B \\ C \end{bmatrix} = \prod_{j=1}^{a} \begin{bmatrix} \cos\delta_j & i\sin\delta_j/\eta_j \\ i\eta_j\sin\delta_j & \cos\delta_j \end{bmatrix} \begin{bmatrix} 1 \\ \eta_{sub} \end{bmatrix} \tag{14}$$

The reflectance can then be written as

$$R = \left(\frac{\eta_0 - Y_e}{\eta_0 + Y_e}\right)^2 \tag{15}$$

Other than the reflectance, we can also design a multi-layer device using the equivalent admittance approach above. When an incident light emits from its surrounding medium onto a multi-layered device with substrate Y_{sub}, we can treat it as if it is moving in a virtual reference plane from the substrate admittance (Y_{sub}), to the front surface of the multi-layer material (see Fig. 2(b)).

The plot of Y_e on the complex plane shows traces of these changes. Plots of these changes are called admittance diagrams or admittance loci [22]. The admittance loci allow us to calculate the reflectance with the oblique incident angle

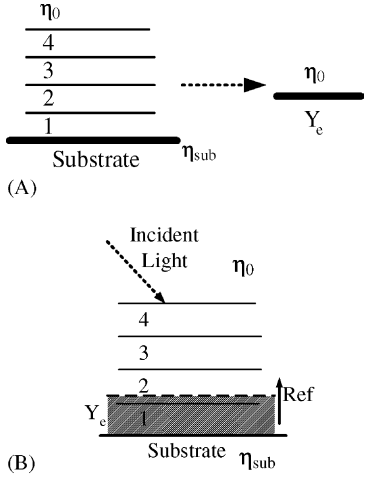

Fig. 2. (a) Equivalent admittance of multi-layer over-coatings, where η_0, η_{sub}, and η_e are the admittance of the surrounding medium, substrate, and equivalent admittance, respectively, and (b) admittance loci treated as if moving a virtual reference plane (Ref) from the substrate admittance (Y_{sub}) to the front surface of the multi-layer.

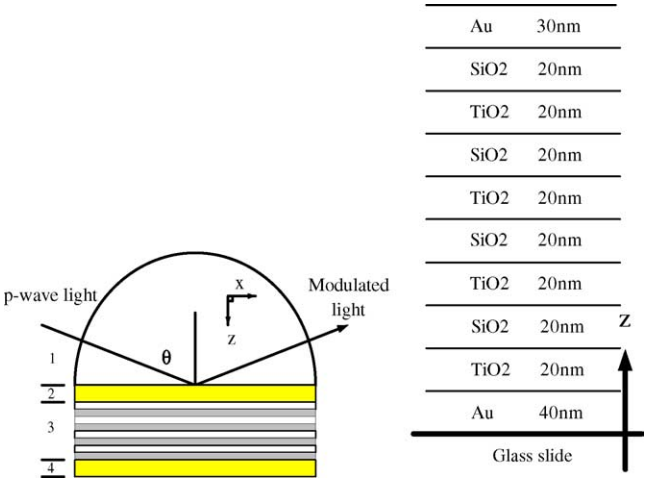

Fig. 3. A proposed model device with symmetrical structure of Au/(SiO_2, TiO_2)$_n$/Au ($n = 4$) for simulation.

(as in conventional SPR design), or with arbitrary structure (as in the multi-layer design).

2.2. Design and simulation

The three major coupling methods for generating SPR signals are prism, fiber, and corrugated grating. Using a prism coupler on a stack of alternative dielectric layers, the perpendicular component of the incident wave will manifest alternating high/low refractive index. With a grating coupler, the transverse electromagnetic wave propagating along the surface of the grating material and the surrounding medium will also manifest alternating high/low refractive index. Although these configurations have been widely used in high-performance anti-reflection or in selective band-pass optical coatings with dielectric mirrors or DBR, they have not been applied to the design of SPR sensors.

Fig. 3 shows a diagram of the multi-layer SPR device we proposed in this paper. The refractive index (n) and extinction coefficient (k) of the multi-layered device used to verify our theoretical calculations are summarized in Table 1. We compared our multi-layer SPR device with a conventional single-layer metallic thin film made of 1 nm Cr/50 nm Au.

Our design goal was to bring the admittance loci at the resonant angle as close to zero reflectance as possible. The number of layers was optimized, given the available materials and their thickness. A simulation program was developed using MATLAB 5.3 (Mathworks Inc., USA). The results were compared with the results obtained using Essential Macleod 8.5 (Thin Film Center Inc., USA.).

Table 1
Optical parameters of materials used for the theoretical calculation and verification

Materials	Refractive index (n)	Extinction coefficient (k)
Glass (BK7)	1.515	0
Au	0.16195	3.20991
SiO_2	1.45705	0
Si (crystal)	4.27	0.57688
TiO_2	2.27892	0.00015
CaF_2 (ir)	1.39672	0.001
H_2O	1.33169	0

2.3. Materials

We used SuperFrost-100 (MENZEL-GLASER, German, refractive index = 1.51), a standard microscopy glass slide, as the substrate for metallic thin film deposition. The metallic thin film used was gold (Au), the high/low refractive index materials used were TiO_2 ($n = 2.28$) and SiO_2 ($n = 1.46$), with Cr for the surface layer. All deposited materials (SiO_2, TiO_2, Cr, Au) used had purity >99.99%. The glucose solutions used were prepared by series dilution of D-(+)-glucose (Sigma, USA) in ddH_2O, with weight percentages of 10%, 20%, and 40%. The refractive indices were measured using KEM RA-130 (Kyoto Electronics, Japan), a refractometer. The obtained n values at room temperature were 1.3484, 1.3644 and 1.3968, respectively.

2.4. Fabrication

The glass slides were cleansed with *piranha* solution (H_2SO_4:H_2O_2 3:1) at 90 °C to remove organic debris. The surface was then immersed in an ultrasonic water bath for 10 min, and cleansed with detergent and acetone. Finally, ethanol and cotton paper were used to thoroughly drain the water.

The sequence of deposition for the Au film was 1 nm of Cr, followed by 50 nm of Au at a pressure of $\sim 1.6 \times 10^{-5}$ torr, in an e-beam evaporator (9 kV). The deposition process was performed at the Precision Instrument Development Center in Hsinchu, Taiwan at 0.1–0.2 nm/s. The thickness of the deposited thin film was monitored using a quartz crystal microbalance (QCM), which was carefully calibrated to the different characteristics of deposited materials. To improve the quality of the thin films and its adherence, the substrate was heated at various temperature during the evaporation of the gold layer (100 °C) and the dielectric layers (300 °C). It is generally known that better results can be obtained when Au and TiO_2 are pre-melted. Hence, this is an essential process in making multi-layered devices.

2.5. Verification

Our multi-layer SPR device was tested on Cary 50 (Varian Inc., USA), a spectrophotometer for spectral measurements in a transmittance mode; EP3 (Nanofilm Inc., Germany), an imaging ellipsometer for optical properties of thin film and SPR spectra. The following equation shows how the measured external angles (θ_{ATRe}) are related to the calculated internal angles (θ_{ATR}):

$$\theta_{ATRe} = \sin^{-1}\left[\sqrt{\varepsilon_0}\sin(\theta_{ATR} - \Psi)\right] + \Psi \quad (16)$$

In our experimental set-up, $\Psi = 45°$.

3. Results and discussion

Position, full-width-at-half-maximum (FWHM), and depth are the three major features of an SPR spectrum. These features are dependent on the incident wavelength, the incident angle, and the dielectric constant of the metallic medium and the dielectric medium. To design a simple and low cost device, we evaluated various combinations of dielectric material and structure. We found that there are many ways to modulate the resonant condition—by using a near infrared light source or using a prism with higher refractive index.

Our SPR design uses dielectric mirrors of alternating high/low refractive index materials, and is based on the theory of distributed Bragg reflector (DBR) for vertical cavity surface emission lasers (VCSELs). In a corrugated grating coupler, the transverse electromagnetic wave propagating along the surface of the grating material and the surrounding medium will manifest alternating high/low refractive index. This method has been widely used in high-performance anti-reflection or selective band-pass optical coatings with dielectric mirrors or DBR. However, it has not been applied in designing SPR sensors.

Our multi-layer SPR device was simulated theoretically using Fresnel's equations for transmittance spectra (400–1200 nm) and SPR spectra (θ_{ATRe} from 40° to 90°). Fig. 4 shows that by tweaking the nanostructure, the FWHM can be improved and resonant angle reduced. This is particularly useful in optical alignment, and in improving spectral resolution.

With a 632 nm-wavelength light source on a BK7 coupling prism, our laboratory tests showed an 11.5° shift in resonant peak position towards the critical angle (from 74° in a conventional single-layer Au film), and a 3.25 times decrease in FWHM (6.18 versus 1.92). Our design also resulted in a wider dynamic range of up to a 1.50 refractive index unit (RIU), compared to a 1.38 RIU in a conventional single-layer Au film. Using glucose solutions in ddH_2O, the calculated resolution was 1.28×10^{-5}. The calculated intensity sensitivity was 10 000 a.u./RIU, about twice the improvement over the conventional single-layer Au film.

During fabrication, the thickness of the deposited materials could deviate by as much as 33% from the quartz crystal microbalance (QCM)-reported number. Deviations in dielectric- or metallic-layer thicknesses shift the peak position and change the peak intensity in the transmittance and SPR curves. To alleviate this problem, we carefully calibrated the QCM responses to different deposited materials.

The TEM image in Fig. 5(a) shows a cross-sectional view of the $(SiO_2/TiO_2)_4$/Au/glass structure. The quality of the thin film is essentially dependent on the condition of the surfaces of the metallic/dielectric media, and fabrication-related variables. For example, a slow deposition rate, along with substrate heating, resulted in stronger bonding and tighter packing density, and consequently, enhancing the overall mechanical stability and increasing resistance to scratch.

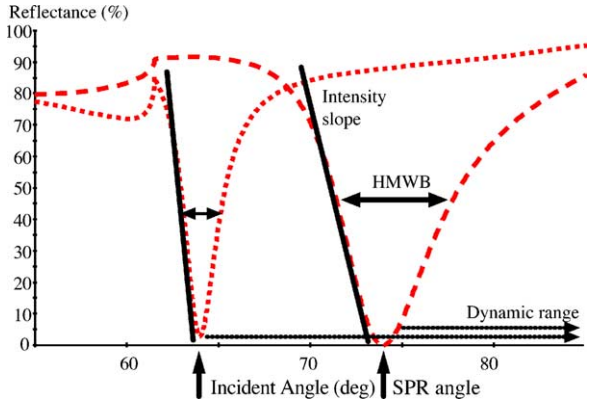

Fig. 4. The simulation results of the proposed model device when compare to a traditional SPR device in water with a BK7 as the coupling prism when illuminated with a 632 nm wavelength light source. *Note:* the results indicate that the newly proposed device has a better performance in terms of FWHM and angle shift towards a smaller resonant angle for easier optical alignment and spectral resolution.

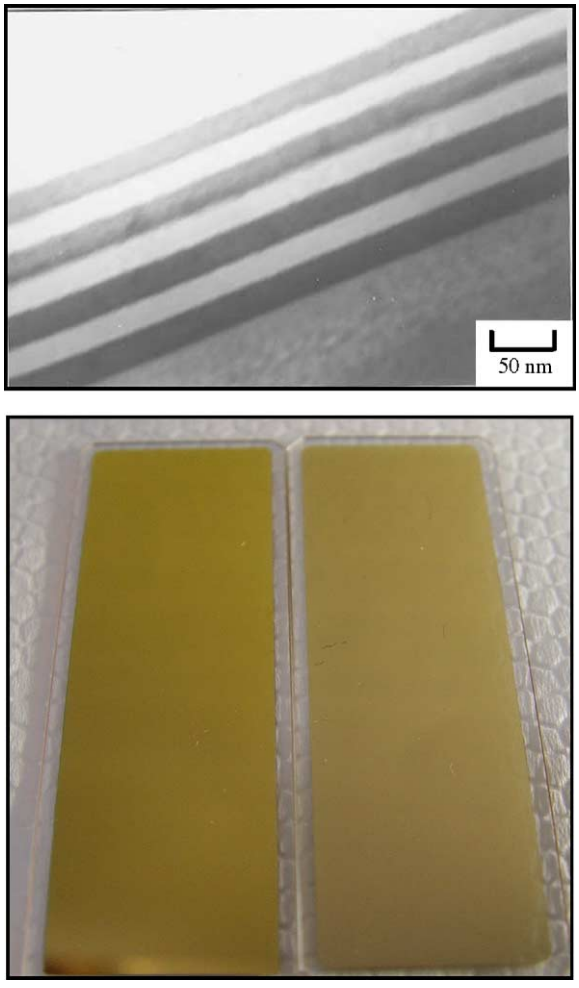

Fig. 5. (a) TEM image of a fabricated device shows the cross-sectional view of a $(SiO_2/TiO_2)_4$/Au/glass structure, and (b) color emergences of the fabricated device (multi-layer right-hand side vs. single-layer left-hand side) were nearly the same in reflective images.

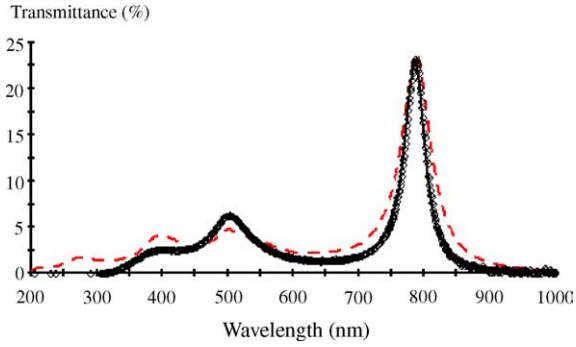

Fig. 6. Measured transmittance spectrum (solid line) of fabricated multi-layer device vs. theoretical calculation (dashed line) in the air. We obtain two major transmission peaks: one at 500 nm and the other at 790 nm, which contribute to their color appearance.

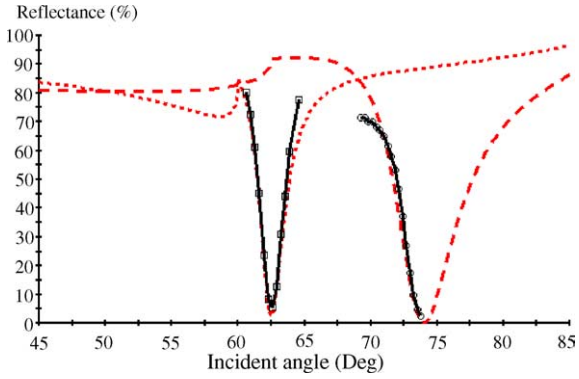

Fig. 7. Reflectance SPR spectra measured (solid line) from fabricated devices (multi-layer as open squares, single-layer as open circles) and from theoretical calculation of both devices (dashed line) in the water with BK7 and 632 nm wavelength light source.

The n and k values of the deposited thin films, measured using ellipsometry, turned out to be slightly different from those of the raw materials. This is partially attributed to the pores and cavities in the deposited thin films. The difference can be used to estimate the packing density (p). For optical thin films, p is typically in the range of 0.75–1.0.

In our test runs, the p values for 20 nm SiO_2 and TiO_2 were 0.96 and 0.82, respectively. The p values for both 30 and 50 nm Au was about 0.98. The p values for the thin films are therefore within the acceptable range.

Fig. 5(b) compares the color emergences of the devices in the air. The picture on the right shows the color emergences of the multi-layer device, and the color emergences of the conventional single-layer Au film is shown on the left. As shown, the color emergences are nearly identical.

The solid line in Fig. 6 shows the measured transmittance spectrum in the air of our multi-layer SPR device. The measured transmittance spectrum agrees well with our theoretical calculations, shown here in dashed line. There are clearly two major transmission peaks: one at 500 nm and the other at 790 nm.

The solid lines in Fig. 7 show the measured SPR spectra, in oblique incidence, under water. Table 2 compares our multi-layer SPR device with a conventional single-layer Au film. Notice that the resonant angle shifted from 73.9° (open circles) to 62.54° (open square). This agrees well with our theoretical calculations for both single-layer (broken lines) and multi-layer (dashed lines) devices. Our test results showed the HMBW decreased from 6.5 to 2. This is a 3.25 times improvement of the damping factor for an interband transition.

Moreover, our multi-layer SPR device showed a wider dynamic range of up to a 1.50 refractive index unit (RIU), compared to the allowable refractive index range of 1.331–1.38 in a conventional single-layer Au film.

Fig. 8 shows the measured refractive indices of our multi-layer SPR device in glucose solutions of weight percentages 0% (ddH_2O), 10% (□), 20% (△), and 40% (◯). The refractive indices measured, at room temperature, using a refractometer were 1.331, 1.3484, 1.3644, and 1.3968, respectively. The corresponding SPR angles were $62.54 \pm 0.021°$,

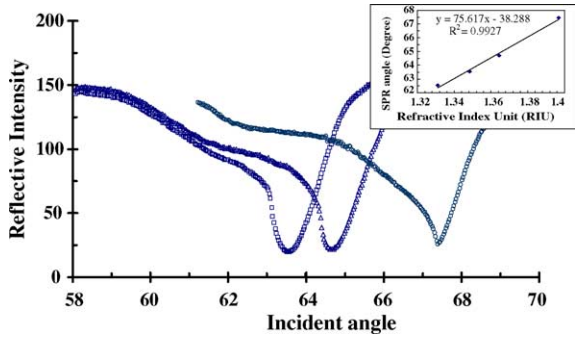

Fig. 8. Measurement results obtained at 10% (□), 20% (△), and 40% (◯) of glucose solutions (in weight percentage). Measured refractive indices under room temperature were 1.331 (ddH_2O), 1.3484, 1.3644, and 1.3968, respectively. The corresponding SPR angles were $62.54 \pm 0.021°$, $63.55 \pm 0.015°$, $64.7 \pm 0.02°$, and $67.46 \pm 0.017°$ ($n = 3$). The linear regression of the calibration curve was $y = 75.617x - 38.288$ with a correlation coefficient $R^2 = 0.9927$, where y is the SPR angle (in °) and x is the refractive index unit (RIU).

Table 2
Performance comparisons of a traditional vs. new SPR device

	SPR angle	HMBW	Dynamic range[a] (RIU)	Resolution[b] ($\times 10^{-5}$ RIU)	Intensity slope[c]	Intensity sensitivity[d]
Single-layer Au	73.9	6.5	1.331–1.38	8.33	58.65	6900
New device	62.54	2	1.331–1.50	1.25	127.5	10000

[a] RIU is the refractive index unit.
[b] Angular measurement of 10^{-3} angular resolution.
[c] Intensity change (0–255)/1° shift.
[d] Intensity change/1 RIU change.

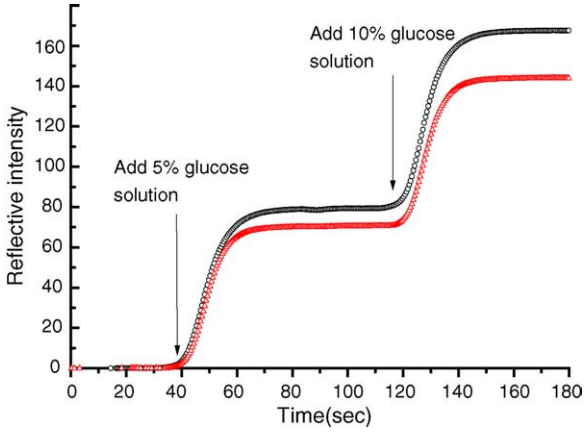

Fig. 9. Reflective intensity measurement at a near resonant angle for real time monitoring of the biochemical signals. New device (◯) shows a shorter transition time and higher steady-state responses when compared to a traditional one (△) at 5% and 10% glucose solutions.

$63.55 \pm 0.015^\circ$, $64.7 \pm 0.02^\circ$, and $67.46 \pm 0.017^\circ$ ($n = 3$), respectively.

The least-square linear regression equation for the calibration curve is $y = 75.617x - 38.288$, with $R^2 = 0.9927$, where y is the SPR angle (in degrees) and x is the refractive index unit (RIU). The high R^2 value indicates a linear relationship between the SPR angle and the refractive index. This has practical application in real time monitoring of biochemical signals—by choosing a reflective intensity measurement at a near resonant angle. Compared with a conventional single-layer Au film (△), our multi-layer SPR device (◯) has a shorter transition time and a higher steady-state response at 5% (74.8 ± 0.22 versus 70.02 ± 0.29) and 10% (165.5 ± 0.16 versus 143.6 ± 0.24) glucose solutions. This is shown in Fig. 9.

The resolution of an SPR sensor is the minimum change in a measured parameter (RIU, thickness, or concentration) that can be resolved by a sensing device. The angular resolution of the instrument used in our laboratory is 0.001 degrees. From our glucose tests, the least-square linear regression equation between the SPR angle change (θ) and concentration (x in weight percentage) is $\theta = 8.021x - 500.36$. The resolution of the angular measurement is therefore 8×10^{-3}% per angle change. The least-square linear regression equation between concentration (x) and RIU (y) is $y = 0.016x + 1.3317$. Hence, the resolution is 1.28×10^{-5} RIU. Since sensitivity is the partial derivative of the SPR intensity parameter with respect to RIU, the calculated intensity slope is 127.5 a.u./°, and the intensity sensitivity is 10 000 a.u./RIU.

4. Summary and conclusions

The principal feature of our SPR design is the use of alternating dielectric layers of dielectric mirrors to enhance the quality of the SPR signal and to modulate its resonant position. The thickness, number of layers, and other design parameters of the material used were optimized using optical admittance loci analysis. A proof-of-concept device was fabricated with a symmetrical structure using $Au/(SiO_2/TiO_2)_4/Au$. The measured transmittance and SPR spectra agreed well with theoretical calculations.

Using a 632 nm-wavelength light source on a BK7 coupling prism, our laboratory tests showed that under water, there is an 11.5° shift in resonant peak position towards the critical angle (from 74° in a conventional single-layer Au film), and a 3.25 times decrease in FWHM (the half-peak width). Our design also resulted in a wider dynamic range of up to a 1.50 refractive index unit (RIU), compared to a 1.38 RIU in a conventional single-layer Au film. Using glucose solutions, the calculated resolution was 1.28×10^{-5}. The calculated intensity sensitivity was 10 000 a.u./RIU, about twice the improvement over the conventional single-layer Au film.

For fine tuning the SPR resonant conditions, we demonstrated that the nano-structure of a dielectric mirror can be represented by an equivalent admittance. Our test results on transmittance, ellipsometry and SPR spectra indicate that our device can be used for various biochemical applications. We can apply this design to biomolecules by treating the biomolecules as dielectric thin films. As part of a plasmon resonance system, biomolecules interact with nano/micro-metallic structures for a specific resonant angle, wavelength, and reflectance. As precision multi-layer optical coatings are relatively low cost, we can apply admittance loci design methodology and use our design as a tool in developing "bio-plasmonics".

Dielectric mirrors of alternating high/low refractive index materials, based on the design of distributed Bragg reflector (DBR) for vertical cavity surface emission lasers (VCSELs), can be used in designing SPR biochemical sensors.

Acknowledgements

This project was supported by the National Science and Technology Program in Pharmaceuticals and Biotechnology, National Science Council, Taiwan, NSC 93-2323-B002-011, NSC 93-2323-B002-017.

References

[1] H. Raether, Excitation of Plasmons and Interband Transitions by Electrons, Springer-Verlag, Berlin, 1980.
[2] H. Raether, Surface Plasmons on Smooth and Rough Surfaces and on Gratings, Springer-Verlag, Berlin, 1988, pp. 4–37.
[3] Z. Salamon, H.A. Macleod, G. Tollin, Surface plasmon resonance spectroscopy as a tool for investigating the biochemical and biophysical properties of membrane protein system. I. Theoretical principles, Biochim. Biophys. Acta 1331 (1997) 117–129.
[4] W.P. Chen, J.M. Chen, Use of surface plasma waves for determination of the thickness and optical constants of thin metallic films, J. Opt. Soc. Am. 71 (1981) 189–191.

[5] K. Kurosawa, R.M. Pierce, S. Ushioda, J.C. Hemminger, Raman scattering and attenuated-total-reflection studies of surface-plasmon polarizations, Phys. Rev. B 33 (1986) 789–798.
[6] J. Homola, S.S. Yee, G. Gauglitz, Surface plasmon resonance sensor: review, Sens. Actuators B 54 (1994) 3–15.
[7] Z. Salamon, H.A. Macleod, G. Tollin, Surface plasmon resonance spectroscopy as a tool for investigating the biochemical and biophysical properties of membrane protein system. II. Applications to biological systems, Biochim. Biophys. Acta 1331 (1997) 131–152.
[8] J.G. Gordon II, S. Ernst, Surface plasmons as a probe of the electrochemical interface, Surf. Sci. 101 (1980) 499–506.
[9] B. Liedberg, C. Nylander, I. Lundstrom, Surface plasmons resonance for gas detection and biosensing, Sens. Actuators 4 (1983) 299–304.
[10] Z. Salamon, M.F. Brown, G. Tollin, Plasmon resonance spectroscopy: probing molecular interactions within membranes, Trends Biochem. Sci. 24 (1999) 213–219.
[11] V. Silin, A. Plant, Biotechnological applications of surface plasmon resonance, Trends Biotechnol. 15 (1997) 353–359.
[12] E. Saenko, A. Sarafanov, N. Greco, M. Shima, K. Loster, H. Schwinn, D. Josic, Use of surface plasmon resonance for studies of protein–protein and protein–phospholipid membrane interactions, J. Chromatogr. A 852 (1999) 59–71.
[13] J. Haimovich, D. Czerwinski, C.P. Wong, R. Levy, Determination of anti-idiotype antibodies by surface plasmon resonance, J. Immunol. Methods 214 (1998) 113–119.
[14] C.Y. Huang, C.-W. Lin, T.S. Kou, An analytical system for multilayer surface plasmon resonance signal, in: Proceedings of the IEEE/EMBS 23rd Annual International Conference, Istanbul, Turkey, 2001.
[15] C.-W. Lin, Y.T. Liu, C.Y. Huang, J.P. Chiu, T.S. Kou, Dual mode fiber optic SPR chemical microsensor, in: Proceedings of SPIE, vol. 4597, ISPA, Singapore, 2001, pp. 151–156.
[16] B.P. Nelson, A.G. Frutos, J.M. Brockman, R.M. Corn, Near-infrared surface plasmon resonance measurements of ultrathin films, Anal. Chem. 71 (1999) 3928–3934.
[17] F.Y. Kou, T. Tamir, Range extension of surface plasmons by dielectric layers, Opt. Lett. 12 (1987) 367–369.
[18] D. Sarid, Long-range surface-plasma waves on very thin metal film, Phys. Rev. Lett. 47 (19811927-1930).
[19] G.G. Nenninger, P. Tobiska, J. Homola, S.S. Yee, Long-range surface plasmons for high-resolution surface plasmon resonance sensors, Sens. Actuators B 74 (2001) 145–151.
[20] Z. Salamon, H.A. Macleod, G. Tollin, Coupled plasmon-waveguide resonators: a new spectroscopic tool for probing proteolipid film structure and properties, Biophys. J. 73 (1997) 2791–2797.
[21] M. Osinski, V.A. Smagley, G.A. Smolyakov, P.G. Eliseev, Design of InGaN-GaN-AlGaN vertical-cavity surface-emitting lasers using electrical–thermal–optical simulation, IEEE J. Quant. Electron. 7 (2002) 270–279.
[22] Thin film optical materials, in: A. Macleod, J. Elshabini-Riad, F.D. Barlow III (Eds.), Thin Film Technology Handbook, McGraw-Hill, New York, 1998 (Chapter 8).

Biographies

Chii-Wann Lin received his BS from Department of Electrical Engineering, National Cheng-Kung University in 1984. He obtained a MS degree from the Institute of Biomedical Engineering, National Yang-Ming University in 1986. After completing a 2-year compulsory military service, he attended Case Western Reserve University where he received his PhD degree in biomedical engineering in January1993. After an 8 month postdoctoral position as a research associate in the Neurology Department at Case Western Reserve University, he joined the Center for Biomedical Engineering, College of Medicine, National Taiwan University in September 1993. Since 1998, he has been an associate professor at the Institute of Biomedical Engineering. Currently, he holds a joint appointment at the Department of Electrical Engineering, National Taiwan University. He is a member of IEEE EMBS, IFMBE and Chinese BMES. His research interests include biomedical micro-sensors, optical biochips, surface plasmon resonance, and nano-medicine.

Kuo-Ping Chen received his BS degree in Electrical and Control Engineering from National Chiao Tung University, Taiwan in 2002. He obtained his MS degree in biomedical engineering from National Taiwan University in 2004. He is currently a research engineer with the Biomedical Engineering Center at Taiwan's Industrial Technology Research Institute (ITRI) working on medical device development. His research interests include surface plasmon resonance, bio-sensor systems, electronics and signal processing.

Chien-Nan Hsiao received his PhD degree in materials science and engineering, National Taiwan University in 2000. He is currently a section manager at the Precision Instrument Development Center (PIDC), National Science Council. His research interests include vacuum technology, thin film technology and phase transformations in materials.

Shiming Lin received his PhD from the Institute of Biotechnology, University of Cambridge, United Kingdom in 1995. He is currently an associate professor at the Center for Optoelectronic Biomedicine, National Taiwan University. His research interests include nano-biotechnology and optoelectronic biotechnology, with a special focus on the molecular biomechanics of protein helix, viral surfaces and biomolecular interaction forces, as well as on the manufacture of optoelectronic bio-sensors and biochips.

Chih-Kung Lee received his PhD degree from Cornell University in 1987. He worked at IBMs Almaden Research Center in San Jose, California for seven years before returning to Taiwan. He is currently director general of engineering and applied sciences at the National Science Council, Taiwan. He is concurrently a professor at the Institute of Applied Mechanics, National Taiwan University, and holds a joint appointment at the Institute of Engineering Sciences and Ocean Engineering, National Taiwan University. He is a fellow of the Institute of Physics.